On Galaxy-Cluster Sizes and Temperatures

Licia Verde[1,2], Marc Kamionkowski[3], Joseph J. Mohr[4,5] & Andrew J. Benson[3,6]

[1] *Institute for Astronomy, University of Edinburgh, Royal Observatory, Blackford Hill, Edinburgh EH9 3HJ, United Kingdom*
[2] *Dept. Astrophysical Sciences, Peyton Hall, Princeton University, Princeton NJ 08544-1001, USA*
[3] *California Institute of Technology, Mail Code 130-33, Pasadena, CA 91125, USA*
[4] *Department of Astronomy and Astrophysics, University of Chicago, 5640 South Ellis Avenue, Chicago, IL 60637-1433, USA*
[5] *Department of Astronomy, University of Illinois, 1002 W. Green, Urbana, IL 61801, USA*
[6] *Physics Department, University of Durham, Science Laboratories, South Road, Durham DH1 3LE, United Kingdom*

28 October 2018

ABSTRACT

We show that the distribution of the sizes and temperatures of clusters can be used to constrain cosmological models. The size-temperature (ST) distribution predicted in a flat Gaussian cluster-abundance-normalized $\Omega_0 = 0.3$ model agrees well with the fairly tight ST relation observed. A larger power-spectrum amplitude σ_8 would give rise to a larger scatter about the ST relation as would a larger value of Ω_0 and/or long non-Gaussian high-density tails in the probability density function. For Gaussian initial conditions, the ST distribution suggests a constraint $\sigma_8 \Omega_0^{0.26} \simeq 0.76$. The ST relation is expected to get tighter at high redshifts. In the process, we derive a simple formula for the halo formation-redshift distribution for non-Gaussian models. We also suggest that the discrepancy between the naive zero-redshift ST relation and that observed may be due, at least in part, to the fact that lower-mass clusters form over a wider range of redshifts. An Appendix derives an equation for the formation-redshift distribution of halos.

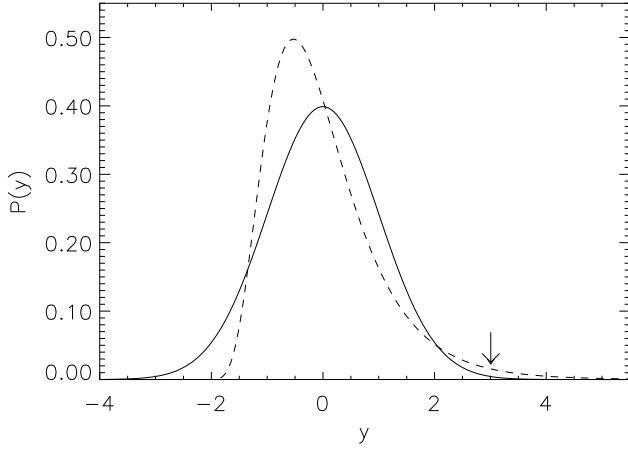**Key words:** cosmology: theory - large scale structures - clusters of galaxies

1 INTRODUCTION

Galaxy clusters are now being widely used as probes of cosmological and structure-formation models. For example, the abundance of galaxy clusters has been used to constrain the amplitude σ_8 of the power spectrum and the nonrelativistic-matter density Ω_0 in models with an initially Gaussian distribution of density perturbations (Evrard 1989; Henry & Arnaud 1991; Bahcall & Cen 1992; Bahcall & Cen 1993; Lilje 1992; Oukbir & Blanchard 1992; White, Efstathiou & Frenk 1993; Viana & Liddle 1996; Eke, Cole & Frenk 1996; Viana & Liddle 1999), as well as in models with long non-Gaussian tails (Robinson, Gawiser & Silk 2000; hereafter RGS).

In this paper, we show that the scatter in galaxy cluster scaling relations can be used to constrain cosmological and structure formation models. Specifically, we focus on the relatively small scatter of the relation between X-ray isophotal size and emission-weighted intracluster-medium mean temperature T_X demonstrated in Mohr & Evrard (1997; hereafter ME97). We illustrate how this scatter should depend on σ_8 and Ω_0, and how it is affected by the introduction of a non-Gaussian distribution of perturbations with a long tail of high-density peaks. Our work on the size-temperature (ST) relation follows prior analytic work by Kitayama & Suto (1996) (although they focussed primarily on other cluster properties) and employs the framework for relating the ST relation to the underlying dark matter properties as discussed in Mohr et al. (2000; hereafter M00).

The small scatter is heuristically expected if clusters form at rare high-density peaks in a Gaussian primordial distribution. Clusters that form earlier should be denser when they are first virialized and so they should have smaller radii for a given mass, or similarly, smaller radii for a given temperature. In this way, any dispersion in the formation redshifts for clusters of a given mass should yield a spread in the ST relation. If clusters come from rare Gaussian peaks, then the spread in formation redshifts should be small; given the rapidly dying Gaussian tails, it is unlikely that any cluster of a given mass observed today was formed at a redshift much earlier than the others. However, if the distribution had long non-Gaussian tails (as would be required to significantly boost the cluster abundance) or if clusters formed from peaks that were not quite so rare (e.g., $> 2\sigma$ rather than $> 3\sigma$ peaks), then clusters of a given mass observed today should have had a much broader distribution of formation redshifts (see Fig. 1) and thus a much broader distribution of sizes (for a given mass or temperature).

We quantify these arguments using a spherical-top-hat-collapse model to relate the virial radius and temperature of a cluster to its mass and formation redshift. We use the formation-redshift distribution for Gaussian perturbations from Sasaki (1994), and we generalize it for an arbitrary initial density distribution (the derivation is presented in an Appendix). We use a Monte Carlo approach to simulate the ST relation for a variety of parameters, and illustrate in particular how it depends on σ_8, Ω_0, and G, the non-Gaussian

Figure 1. The solid curve shows a Gaussian distribution $P(y)$ with unit variance, while the broken curve shows a non-Gaussian distribution with the same variance but 10 times as many peaks with $y > 3$. This illustrates (a) how the cluster abundance can be dramatically enhanced with long non-Gaussian tails (since clusters form from rare peaks); and (b) that the dispersion of y for $y > 3$ is much larger for the non-Gaussian distribution than it is for the Gaussian distribution, and this will lead to a larger scatter in the formation redshifts and sizes of clusters of a given mass.

Figure 2. Mass and formation-redshift contours in the size-temperature plane for $\Omega_0 = 0.3$ and $h = 0.65$ obtained from the spherical-top-hat model of gravitational collapse discussed in the text. It is clear from the figure that a narrow (broad) spread in the formation redshift will yield a tight (broad) ST relation. For larger Ω_0, the $z_f = 0$ contour remains the same, but the spacing between equi-z_f contours increases.
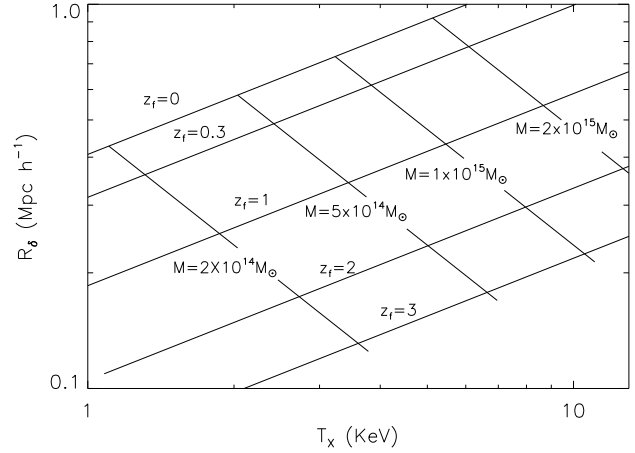
multiplicative excess of $> 3\sigma$ peaks introduced by RGS. Our main results are (a) the predicted scatter in the ST relation for Gaussian initial conditions and favored cosmological parameters is found to be fairly consistent with that observed; (b) $G \gtrsim 5$ greatly over-predicts the scatter; (c) the scatter for the non-Gaussian initial conditions required to make the cluster abundance consistent with an Einstein-de-Sitter Universe (EdS) is also much larger than that observed. Joint constraints from the cluster abundance and the ST relation on σ_8, G, and Ω_0 are discussed. We show how the ST relation should be altered for clusters at intermediate and high redshifts. In the process we show that, because lower-mass clusters form over a larger range of redshifts than higher-mass clusters, the expected ST relation is steeper (and therefore more consistent with the observed relation) than the naive expectation detailed in M00. In the final Section, we make some brief connections to the X-ray mass-temperature relation and to the redshift evolution of the cluster abundance.

2   INGREDIENTS

2.1   Spherical-Collapse Model

We use the relations of Kitayama & Suto (1996) to relate the cluster virial radius and virial temperature at formation time, $R_{\rm vir}$ and T, to the mass M and formation redshift z_f (defined to be the redshift at which the cluster collapses). Fig. 2 shows how this model assigns masses and formation redshifts to clusters of given temperatures and sizes assuming that $R_{\rm vir} \propto R_\delta$.

It is possible to connect more rigorously these cluster dark-matter properties with the observable intracluster medium (ICM) properties in a manner similar to that outlined in M00. Specifically, we assume that T_X is the virial temperature (e.g. Evrard, Metzler & Navarro 1996; Frenk et al. 2000; Bower et al. 2000). We transform from the virial radius at z_f to the X-ray isophotal size R using $R \propto R_{\rm vir}^{4/3} f_{ICM}^{2/3}$, where f_{ICM} is the ICM mass fraction (M00 eqns. (8) and (10)). The dependence on f_{ICM} should be included

because variations in f_{ICM} with mass are observed (e.g. Mohr, Mathiesen & Evrard 1999; David, Jones & Forman 1995) and could alter the slope of the ST relation. In the following analysis, we assume $f_{ICM} \propto T_X^{0.34}$; however the results of Figs. 4 and 5 are no more than *very weakly* dependent on the f_{ICM} functional form.

We normalize the simulated ST relation to the observations by fixing the constant of proportionality so that no observed cluster in the local sample lies above the $z_f = 0$ line (see Figs 2 and 3).

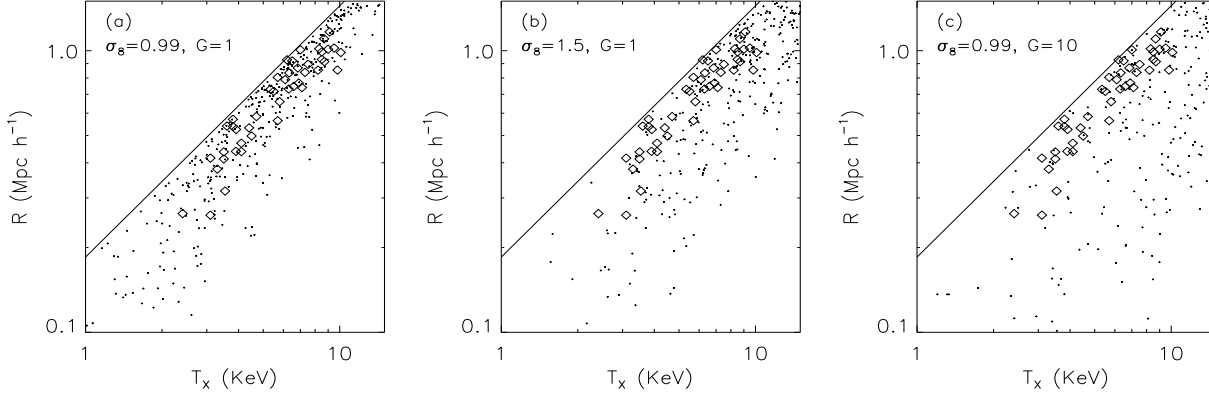### 2.2   Distribution of Halo Masses

Numerical simulations tell us that the Press-Schechter (PS) approach (Press & Schechter 1974) provides a reasonable approximation for the abundance of cluster size halos of a given mass at any given epoch for Gaussian initial conditions (e.g. Lacey & Cole 1994, Gross et al. 1998, Lee & Shandarin 1999), and for a few non-Gaussian initial conditions that have been explored with simulations (Robinson & Baker 1999). In the PS approach the number per comoving volume of halos with masses between M and $M + dM$ at redshift z is (e.g., Lucchin & Matarrese 1988; RGS),

$$\frac{dn}{dM}\,dM = \frac{f\rho_b}{M} P\Big(y(M,z)\Big)\frac{\partial y(M,z)}{\partial M}\,dM, \qquad (1)$$

where ρ_b is the background density, $P(y)$ is the primordial probability distribution function normalized to unit variance. The argument $y = \delta(z)/\sigma_M$, and $\delta(z) = \delta(z)/D(z)$ where $\delta_c(z)$ is the critical overdensity for collapse (see Kitayama & Suto 1996 for accurate analytic fits), and $D(z)$ is the linear-theory growth factor. Here, σ_M is the current root-variance of spheres that enclose an average mass M, and $f = \int_0^\infty P(y)\,dy$.

2.3   Distribution of Formation Redshifts

The objects of mass M observed at some given redshift z_o underwent collapse at a variety of formation redshifts $z_f > z_o$. Sasaki (1994) has shown how the PS formalism leads to an expression for the formation-redshift distribution under the assumption of Gaussian initial conditions and that the merger rate has no characteristic

Figure 3. (a) ST distribution for LCDM and $\sigma_8 = 0.99$ and Gaussian initial conditions. Each dot represents a simulated cluster, while the diamonds are data from M00. The line shows the ST relation expected for clusters that form today, at redshift $z = 0$. (b) shows the same except that here we use $\sigma_8 = 1.5$. (c) shows the same as in (a) but with the non-Gaussian distribution of RGS with $G = 10$.

mass scale. His derivation can be generalized in a straightforward fashion to arbitrary $P(y)$. Doing so (see Appendix), we find the distribution (normalized to unity) of formation redshifts z_f for halos of mass M observed at redshift z_o to be,

$$\frac{df}{dz_f} = P'\big(y(M, z_f)\big) \frac{\partial y(M, z_f)}{\partial z_f} \left[P\big(y(M, z_0)\big) \right]^{-1} \qquad (2)$$

where $P'(y) \equiv dP/dy$. Lacey & Cole (1993,1994) have presented an alternative, but somewhat more complicated, formation-redshift distribution that improves upon Sasaki's assumption of self-similar merging. We will leave the implementation of this alternative distribution and a discussion of the formalism introduced by Percival et al. (2000), to future work, but note that our preliminary investigations, as well as previous results (Viana & Liddle 1996; Buchalter 2000), indicate that the predictions of these models do not differ considerably for cluster-mass halos.

2.4 Preliminary Estimates

It is straightforward to roughly estimate the effects of non-Gaussian tails on the ST-relation scatter. For a rapidly dying distribution $P(y)$, the controlling factor in dn/dz_f will be $P'(y)$. For a Gaussian $P(y)$, the root-variance of y is 0.282 for the distribution $P'(y)$ for values of $y > 3$, and the mean value of y is 3.30. For an EdS model, $y = 1.69(1 + z_f)/\sigma_M$, and $(1 + z)^{-1} \propto R_{\rm vir}$. Thus, $\sigma_R/R = (4/3)(\sigma_{R_{\rm vir}}/R_{\rm vir}) \simeq (4/3)(\sigma_y/y) = 0.113$ for a Gaussian distribution, in surprisingly good agreement with the estimate of the intrinsic scatter of 10% in the ST relation (ME97). For the RGS distribution with $G = 10$, the root-variance is 0.896 and the mean value of y is 3.87 leading to $\sigma_{R_{\rm vir}}/R_{\rm vir} \simeq 0.31$, more than twice the observed scatter. Below we will quantify this far more precisely.
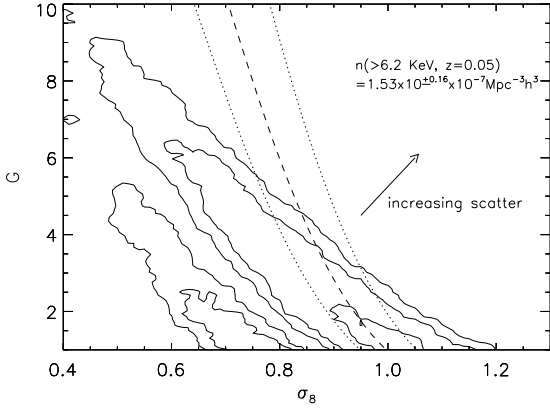
3 RESULTS

For any given Ω_0, σ_8, and G, we perform a Monte Carlo realization of 400 clusters with the mass and formation-redshift distributions given above. We then assign to each of these clusters a size and temperature as outlined in Section 2.1. The ME97 sample to which we compare our calculations is a flux-limited sample. Within this

sample, the probability of finding a cluster of luminosity L_X goes as $L_X^{1.5}$, and L_X is observed to go as roughly $T^{2.5}$ to T^3 (David et al. 1993; Arnaud & Evrard 1999), so the flux limit is essentially a virial-temperature weighting of $T^{3.75}$ to $T^{4.5}$. We thus subject our simulated population of clusters to a $T^{3.75}$ weighting; our results are not significantly altered for the steeper weighting $T^{4.5}$.

Fig. 3(a) shows the results of our Monte Carlo for a flat $\Omega_0 = 0.3$ model (LCDM) with the value $\sigma_8 = 0.99$ inferred from the cluster abundance (Viana & Liddle 1999) and a Gaussian distribution. The data points from ME97 are overlaid. We used a Hubble parameter $h = 0.65$, but the results are essentially unaltered for different plausible values of h. Fig. 3(b) illustrates that the scatter in the ST relation is increased if the power-spectrum normalization is higher. In this case, clusters are not quite as rare, and they form over a larger range of redshifts. Fig. 3(c) shows how the scatter is increased as the abundance of high-density peaks is increased. In this case, clusters observed today are also formed over a broader range of redshifts. At this point, we note the apparent similarity between the predictions of the ST distribution of the cluster-abundance-normalized Gaussian LCDM model and the data; the scatter about the ST relation would be broadened considerably with a higher σ_8 or with a highly non-Gaussian model.

To make these arguments more quantitative as well as survey a larger range of parameters, we have simulated ST relations for a variety of models in the σ_8-G parameter space for both EdS and LCDM models and then used a 2D Kolmogorov-Smirnov (KS) test (Peacock 1983; Press et al. 1996) to compare these with the data. Fig. 4 shows the resulting contours of constant KS significance levels for both $\Omega_0 = 0.3$ and $\Omega_0 = 1$. The results suggest that the Gaussian cluster-abundance-normalized ($\sigma_8 = 0.99$) LCDM model provides a good fit to the data.

We heuristically expect that the dependence of the ST scatter on cosmological parameters/models should be similar to that of the cluster abundance; if the peaks that give rise to clusters are rare, we expect little scatter and *vice versa* if clusters are more common. The contours of fixed cluster abundance in Fig. 4 indicate that this is qualitatively correct. We obtain these curves by using a cluster abundance $n(> 6.2\,{\rm keV}, z = 0.05) = 1.53 \times 10^{\pm 0.16} \times 10^{-7}\,{\rm Mpc}^{-3}\,h^3$ (Viana & Liddle 1999) and integrating eqn. (1) up from the mass associated with a temperature 6.3 keV and a formation redshift $z_f = 0$. However, the detailed results also seem to

Figure 4. The heavy solid curves show confidence levels suggested by the ST data in the σ_8-G parameter space for the LCDM model, and the light curves show the same for the EdS model. The dashed curve shows the contour suggested by the central value $[n(> 6.2\,\mathrm{keV}, z = 0.05) = 1.53 \times 10^{\pm 0.16} \times 10^{-7}\,\mathrm{Mpc}^{-3}\,h^3]$ of the local cluster abundance for $\Omega_0 = 0.3$, while the dotted curves indicate contours for the upper and lower observational limits to the cluster abundance.
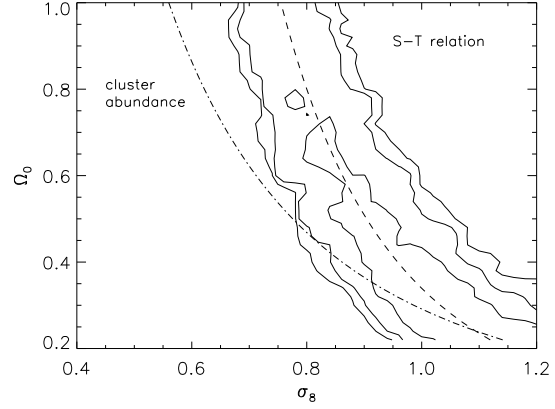
indicate that if Ω_0 is fixed, the ST distribution and cluster abundance can be used in tandem to break the degeneracy between G and σ_8. In fact, combining the two constraints already seems to rule out large deviations from Gaussianity.

Fig. 5 shows the regions of σ_8-Ω_0 parameter space preferred by the ST relation, as well as the curve in this parameter space suggested by the cluster abundance. For fixed σ_8, the ST scatter increases as Ω_0 increases. At first, this might seem discrepant with the well-known result that the range of formation redshifts is narrower for larger Ω_0 for cluster-abundance-normalized models. However, this narrowing of the formation-redshift distribution with increasing Ω_0 is not quite as dramatic if we fix σ_8 instead of the cluster abundance. More importantly, the spherical-top-hat collapse dynamics leads to a broader spacing between the equi-z_f contours in Fig. 2, and this is responsible for increasing the ST scatter as Ω_0 is increased with fixed σ_8; in other words, the relationship between R and T evolves more rapidly with redshift in higher Ω_0 models.
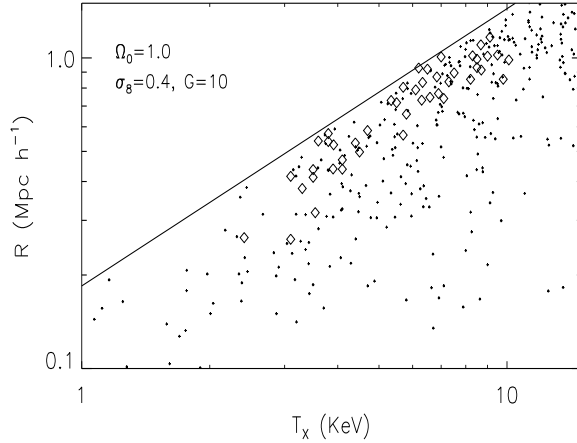
From the results in Fig. 5, we can approximate an ST constraint, $\sigma_8 = 0.76\,\Omega_0^{-0.26}$, as compared with the cluster-abundance constraint, $\sigma_8 = 0.56\,\Omega_0^{-0.47}$ (Viana & Liddle 1999). The region of overlap between the cluster-abundance constraint and the ST relation lies at low values of Ω_0, low values of non-Gaussianity, and slightly higher values of σ_8.

3.1 An Einstein-de-Sitter Universe?

RGS were able to identify for an EdS model, a region in the σ_8-G parameter space near $\sigma_8 = 0.4$ and $G = 10$ in which the predicted cluster abundance was found to agree with that observed. Fig. 6 shows that these parameter choices predict far too much scatter in the ST relation. Allowing for additional sources of scatter in this simulated ST relation would only increase the discrepancy between the model and the observations.

Figure 5. The heavy solid curves show likelihood contours suggested by the ST data for Gaussian initial conditions in the σ_8-Ω_0 parameter space. The dot-dashed curve shows the contour preferred by the local cluster abundance as suggested by Viana & Liddle (1999), while the dashed curve shows the fit to our ST constraint.
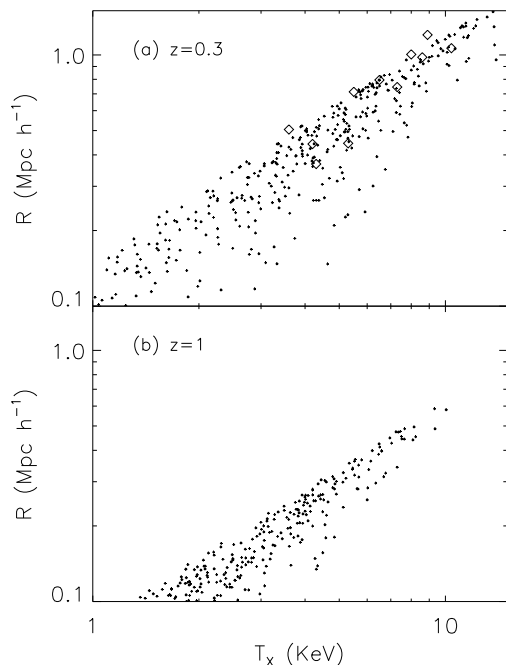

Figure 6. The ST distribution for $\Omega_0 = 1$ with $\sigma_8 = 0.4$ and $G = 10$, one of the combinations of parameter values that yield the correct cluster abundance for an EdS Universe. The predicted scatter in the ST relation is considerably larger than that observed.

3.2 High and Intermediate Redshift Results

Clusters that exist at higher redshifts must form from even higher-density peaks than those today. Thus, in a Gaussian model, the scatter in their formation redshifts and thus in their sizes should be even smaller. This is illustrated in Fig. 7. The canonical-model predictions shown in Fig. 7(a) for $z \simeq 0.3$ seem to be in relatively good agreement with the cluster sample observed so far. Fig. 7(b) shows that the scatter in the ST relation for the canonical model should be *very* small. Even though the sample of such high-redshift clusters is expected to be small, the predicted scatter is so small that measurement of the sizes of only a handful of clusters could put strong constraints on different sources of scatter (e.g., non-Gaussianity, measurement uncertainties, mergers, galaxy feedback, etc.).

3.3 A size-temperature anomaly?

The ST relation of the low-redshift X-ray flux limited cluster sample has a slope of $m \sim 1$, which is considerably steeper than the

Figure 7. The ST relation for the LCDM model with $\sigma_8 = 0.99$ and Gaussian perturbations for (a) clusters at $z = 0.3$ and (b) $z = 1$. This illustrates how the scatter should decrease with redshift. The data from Mohr et al. (2000) (that have median redshift 0.3, but cover the range $0.19 < z < 0.54$) are shown in (a).

$m = 2/3$ slope expected in a model where all clusters are assumed to have formed at the redshift of observation (ME97, M00). ME97 suggest that a possible explanation for this steeper than expected scaling relation is provided by galaxy feedback. Fig. 3 illustrates that the discrepancy may be due only, or at least in part, to the fact that lower-mass clusters form over a broader range of redshifts, and thus will in general have smaller sizes than they would if they all formed very recently. Visual inspection of Fig. 3 suggests that this is a plausible explanation, especially when the small-number statistics of the observational sample are taken into account. Moreover, the relatively strong dependence of the ST scatter on σ_8 indicate that better agreement than shown in Fig. 3 could be obtained with a slightly different value of σ_8 and/or Ω_0 (cf., Fig. 5). The apparent disagreement with ME97's feedback-free numerical simulations, which show an ST scaling close to the naive scaling (but still steeper in 3 of the 4 cosmologies tested), may have been due to this σ_8 and Ω_0 dependence and/or the relatively small-number statistics of their simulations sample. Thus, the apparent deviation of the ST relation slope from the $m = 2/3$ expectation is not quite so anomalous.

4 DISCUSSION

We have calculated the ST distribution of clusters with a simple analytic model and focussed in particular on the dependence on the power-spectrum amplitude (σ_8) and the degree of non-Gaussianity (G). We find a fairly sensitive dependence of the ST relation scatter on these two parameters. Thus, the tightness of the ST relation can be used to place valuable constraints on these parameters, as well as on other cosmological parameters. The canonical cluster-abundance-normalized $\Omega_0 = 0.3$ model predicts an ST relation consistent with that observed, but a σ_8 much larger or smaller would be inconsistent as would a non-Gaussian model that predicts

a significant excess of $> 3\sigma$ high-density peaks.[★] The constraints to σ_8, G, and Ω_0 that arise from the ST distribution should be qualitatively similar to those from cluster abundances, but our preliminary calculations suggest that they may be sufficiently different to provide complementary constraints. The ST relation should become increasingly tight at larger redshifts. Our results also suggest that the discrepancy between the naive $z = 0$ ST relation and the observed ST relation may be due, at least in part, to the fact that lower-mass clusters observed today have formed over a larger range of redshifts than higher mass clusters.

The fact that lower-mass clusters tend to form over a broader redshift range than higher-mass clusters will also tend to steepen the M_{vir}-T relation beyond the self-similar expectation of $m = 2/3$. Numerical simulations of structure formation within models with non-Gaussian initial conditions or low-Ω_0 open models ought to exhibit this effect. The OCDM256 portion of Fig 4. in Bryan & Norman (1998) indicates that low-mass clusters fall systematically below the best fit M_{vir}-T relation, consistent with our expectation. It should be emphasized that, in this particular study, the low-mass systems are composed of far fewer particles than the high-mass systems, providing another plausible explanation for structural differences. Further work to investigate departures from self similarity in the cluster population which naturally arise from the spread in formation epochs is clearly required.

Since the overdensity-peak amplitude at which a cluster can form increases at higher redshift, the redshift evolution of the cluster abundance depends on the shape of the primordial density distribution function at high peaks just as the ST scatter does. Thus, if Ω_0 is fixed, it should be possible to reconstruct the cluster-abundance evolution from the scatter in the ST relation for local clusters.

Although we have used cluster sizes inferred from X-rays to compare with theoretical calculations, the same could be done for the sizes of clusters measured via the Sunyaev-Zeldovich effect, either with or without redshift information (Kamionkowski et al. 2000). Of course, there will invariably be some cluster-formation physics that our current analysis has left out, and numerical simulations may have an advantage in this regard. Note that the only source of scatter in our simulated ST relations is the range of formation epoch, whereas other sources of stochasticity (e.g., measurement uncertainties, mergers, galaxy feedback, etc.) might increase the scatter. However, with our analytic approach, we are able to rule out models that overpredict the scatter; we can sift far more rapidly through a variety of cosmological models and parameters, study the dependence of the ST distributions on these models and parameters, and gain some intuitive feel for how the results arise. By doing so, we hope to have established that cluster sizes can provide a valuable new probe of cosmological models.

★ However, small deviations from Gaussianity have huge impact on clusters at $z_o \gg 0$ (e.g., Matarrese, Verde & Jimenez 2000); for example the small non-Gaussinanity (e.g. $G \simeq 2$) required to accommodate the existence of the MS1054-03 cluster within the LCDM model (Verde et al. 2000b) is consistent with the ST constraint.

APPENDIX

Taking the derivative of eqn. (1) with respect to redshift, we obtain (hereafter we do not explicitly show the (M, z) dependencies where they are obvious)

$$\frac{\mathrm{d}^2 n}{\mathrm{d}M\mathrm{d}z} = \frac{f\rho_b}{M}\left[\frac{\partial P}{\partial y}\frac{\partial y}{\partial z}\frac{\partial y}{\partial M} + P(y)\frac{\partial}{\partial z}\frac{\partial y}{\partial M}\right] \quad (3)$$

$$= -\frac{f\rho_b}{M}\frac{1}{\sigma^2}\frac{\partial\delta}{\partial z}\frac{\partial\sigma}{\partial M}\left[\frac{\partial P}{\partial y}\frac{\delta}{\sigma} + P(y)\right] \quad (4)$$

$$= \frac{\mathrm{d}^2 n_{\mathrm{form}}}{\mathrm{d}M\mathrm{d}z} - \frac{\mathrm{d}^2 n_{\mathrm{dest}}}{\mathrm{d}M\mathrm{d}z}. \quad (5)$$

In the last line we have equated the total rate of change to the difference between a formation rate and a destruction rate (the latter being due to objects merging to form larger objects). These can be expressed as

$$\frac{\mathrm{d}^2 n_{\mathrm{form}}}{\mathrm{d}M\mathrm{d}z} = \int_{M_{\mathrm{min}}}^{M}\frac{\mathrm{d}n}{\mathrm{d}M}Q(M, M'; z)\mathrm{d}M', \quad (6)$$

where $Q(M, M'; z)$ is the probability that an object of mass M' is one of the merging components when an object of mass M forms and M_{min} is introduced to prevent the integral from diverging, and $\mathrm{d}^2 n_{\mathrm{dest}}/\mathrm{d}M\mathrm{d}z = \phi(M, z)(\mathrm{d}n/\mathrm{d}M)$, where the function $\phi(M, z)$ can be interpreted as the destruction rate per bound object. Sasaki assumes that $\phi(M, z)$ can be expressed as $\phi(M, z) = M^{\alpha}\tilde{\phi}(z)$ (implying that the destruction rate has no characteristic mass scale). Using eqn. (5), we can write

$$\tilde{\phi}(z) = \frac{-\mathrm{d}^2 n/\mathrm{d}M\mathrm{d}z + \mathrm{d}^2 n_{\mathrm{form}}/\mathrm{d}M\mathrm{d}z}{\mathrm{d}n/\mathrm{d}M M^{\alpha}}. \quad (7)$$

Since the left-hand side of this equation depends only upon z the right-hand side must be independent of M and so may be evaluated at a very small mass M_{min}. Since the formation rate is zero at M_{min} (see eqn. 6), this leaves

$$\tilde{\phi}(z) = -\frac{\mathrm{d}^2 n/\mathrm{d}M\mathrm{d}z(M_{\mathrm{min}}, z)}{\mathrm{d}n/\mathrm{d}M(M_{\mathrm{min}}, z)M_{\mathrm{min}}^{\alpha}}. \quad (8)$$

Substituting eqns. (1) and (4) into this expression gives

$$\tilde{\phi}(z) = \frac{1}{\delta}\frac{\partial\delta}{\partial z}M_{\mathrm{min}}^{-\alpha}\left[\frac{1}{P[y(M_{\mathrm{min}})]}\frac{\partial P[y(M_{\mathrm{min}})]}{\partial y}\frac{\delta}{\sigma(M_{\mathrm{min}})} + 1\right] \quad (9)$$

For a hierarchical clustering model, $\lim_{M\to 0}\sigma^2(M) = \infty$, so if we take the limit $M_{\mathrm{min}} \to 0$ eqn. (9) will be 0 or ∞ unless $\alpha = 0$, forcing the choice $\alpha = 0$ upon us such that $\tilde{\phi}(z) = (1/\delta)(\mathrm{d}\delta/\mathrm{d}z)$. Substituting this expression and eqn. (3) into eqn. (5), we find that the formation rate is given by

$$\frac{\mathrm{d}^2 n_{\mathrm{form}}}{\mathrm{d}M\mathrm{d}z} = -\frac{f\rho_b}{M}\frac{1}{\sigma^2}\frac{\partial\delta}{\partial z}\frac{\partial\sigma}{\partial M}\frac{\partial P}{\partial y}\frac{\delta}{\sigma}. \quad (10)$$

This is the rate of formation of bound objects of mass M and redshift z, but we wish to know what fraction of these objects will survive until the redshift of observation. Using our definition of $\phi(z)$ the number of objects of mass M which formed at z_{f} must

evolve with redshift as $\mathrm{d}N/\mathrm{d}z = \phi(M, z)N$ such that the fraction remaining by $z_{\mathrm{o}}(< z_{\mathrm{f}})$ is $f(z_{\mathrm{f}}, z_{\mathrm{o}}) = \exp\int_{z_{\mathrm{f}}}^{z_{\mathrm{o}}}\phi(z)\mathrm{d}z = \delta(z_{\mathrm{o}})/\delta(z_{\mathrm{f}})$. The number of objects of mass M, which formed at redshift z_{f} and which survive until redshift z_{o} is given by the product of this expression and eqn. (10); i.e.,

$$\frac{\mathrm{d}^2 n}{\mathrm{d}M\mathrm{d}z} = \frac{f\rho_b}{M}\frac{\delta(z_{\mathrm{o}})}{\delta(z_{\mathrm{f}})}\frac{\partial y}{\partial z}(z_{\mathrm{f}})\frac{\partial y}{\partial M}(z_{\mathrm{f}})\frac{\partial P}{\partial y}(z_{\mathrm{f}}). \quad (11)$$

Noting that $(\partial y/\partial M)_{z_{\mathrm{f}}}/(\partial y/\partial M)_{z_{\mathrm{o}}} = \delta(z_{\mathrm{f}})/\delta(z_{\mathrm{o}})$, we obtain our final result, eqn. (2), by dividing eqn. (11) by eqn. (1).

REFERENCES

Arnaud M., Evrard A. E., 1999, MNRAS, 305, 631
Bahcall N., Cen R., 1992, ApJ, 398, L81
Bahcall N., Cen R., 1993, ApJ, 407, L49
Bahcall N., Fan X., 1998, ApJ, 504, 1
Bower R. G., Benson A. J., Baugh C. M., Cole S., Frenk C. S., Lacey C. G., astro-ph/0006109
Bryan G. L., Norman M. L., 1998, ApJ, 495, 80
Buchalter A., 2000, private communication
David L. P., Slyz S. C., Forman W., Vrtilek S. D., Arnaud K. A., 1993, ApJ, 412, 479
David L.P., Jones C., Forman W., 1995, ApJ, 445, 578
Eke V. R., Cole S., Frenk C. S., 1996, MNRAS, 282, 263
Evrard A. E., 1989, ApJ, 341, L71
Evrard A. E., Metzler C. A., Navarro, J. 1996, ApJ, 469, 494
Frenk et al., 2000, ApJ, in press (astro-ph/9906160)
Gross M. A. K., Somerville R. S., Primack J. R., Holtzman J., Klypin A., 1998, MNRAS, 301, 81
Henry J. P., Arnaud K. A., 1991, ApJ, 372, 410
Jones C., Forman W., 1984, ApJ, 276, 38
Kamionkowski M. et al., 2000, in preparation
Kitayama T., Suto Y., 1996, ApJ, 469, 480
Lacey C., Cole S., 1993, MNRAS, 262, 627
Lacey C., Cole S., 1994, MNRAS, 271, 676
Lee J., Shandarin S., 1999, ApJ, 517, 15
Lilje P. B., 1992, ApJ, 386, L33
Lucchin F., Matarrese S., 1988, ApJ, 330, 535
Matarrese S., Verde L., Jimenez R., 2000, ApJ, 541, 10
Mohr J. J., Evrard A. E., 1997, ApJ, 491, 38 (ME97)
Mohr J. J., Mathiesen B., Evrard A. E., 1999, ApJ, 517, 627
Mohr J. J., Reese E. D., Ellingson E., Lewis A. D., Evrard A. E., 2000, ApJ, 544, in press (astro-ph/0004242)
Oukbir J., Blanchard A., 1992, A&A, 262, L21
Peacock J., 1983, MNRAS, 202, 615
Percival W., Miller L., Peacock J. A., 2000, astro-ph/0002328
Press W. H., Schechter P., 1974, ApJ, 187, 425
Press W. H., Teukolsky S. A., Vetterling W. T., Flannery B. P., 1996, Numerical Recipes (Cambridge University Press, Cambridge)
Robinson J., Baker J. E., 1999, astro-ph/9905098
Robinson J., Gawiser E., Silk J., 2000, ApJ, 532, 1 (RGS)
Sasaki S., 1994, Publ. Astron. Soc. Japan, 46, 430
Verde L., Wang L., Heavens A. F., Kamionkowski M., 2000a, MNRAS, 313, 141
Verde L., Jimenez R., Kamionkowski M., Matarrese S., 2000b, to be submitted to MNRAS
Viana P. T. P., Liddle A. R., 1996, MNRAS, 281, 323
Viana P. T. P., Liddle A. R., 1999, MNRAS, 303, 535

White S. D. M., Efstathiou G., Frenk C. S., 1993, MNRAS, 262, 1023